PNAS

Targeted demethylation and activation of *NLRC5* augment cancer immunogenicity through MHC class I

Xin Sun[1], Toshiyuki Watanabe[1], Yoshitaka Oda[2], Weidong Shen[3], Alaa Ahmad[1], Ryota Ouda[1], Paul de Figueiredo[4,5,6,7], Hidemitsu Kitamura[3,8], Shinya Tanaka[2,9], Koichi S. Kobayashi[1,4,10] *

[1]Department of Immunology, Graduate School of Medicine, Hokkaido University; Sapporo 060-8638, Japan.
[2]Department of Cancer Pathology, Graduate School of Medicine, Hokkaido University; Hokkaido, Sapporo 060-8638, Japan.
[3]Division of Functional Immunology, Section of Disease Control, Institute for Genetic Medicine, Hokkaido University; Sapporo 060-8638, Japan.
[4]Department of Microbial Pathogenesis and Immunology, Texas A&M Health Science Center; Bryan 77807, TX, USA.
[5]Department of Molecular Microbiology and Immunology, University of Missouri School of Medicine; Columbia, MO, 65211 USA.
[6]Christopher S. Bond Life Sciences Center, University of Missouri, Columbia, MO, 65211 USA.
[7]Department of Veterinary Pathobiology, University of Missouri School of Veterinary Medicine, Columbia, MO 65211 USA
[8]Department of Biomedical Engineering, Faculty of Science and Engineering, Toyo University; Kawagoe, Japan.
[9]Institute for Chemical Reaction Design and Discovery (WPI-ICReDD), Hokkaido University; Sapporo 001-0021, Japan.
[10]Hokkaido University, Institute for Vaccine Research and Development (HU-IVReD); Sapporo 060-8638, Japan.

* Corresponding author: Koichi S. Kobayashi, M.D., Ph.D.
Email: kskobayashi@med.hokudai.ac.jp, kobayashi@tamu.edu

Author Contributions: Conceptualization: X.S., T.W., K.S.K.; Methodology: All authors.; Investigation: X.S., T.W., Y.O., A.A.; Visualization: X.S., Y.O.; Funding acquisition: K.S.K., T.W.,

R.O.; Project administration: X.S., K.S.K.; Supervision: K.S.K.; Writing – original draft: X.S., K.S.K.; Writing – review and editing: All authors

Competing Interest Statement: Authors declare that they have no competing interests.

Classification: Biological Sciences; Immunology and Inflammation

Keywords: Cancer immunotherapy; antigen presentation; Immune checkpoint blockade; MHC-I; epigenetic modification.

This PDF file includes:

Main Text

Reference list

Figure legends 1 to 6

Abstract

Impaired expression of MHC (Major histocompatibility complex) class I in cancers constitutes a major mechanism of immune evasion. It has been well documented that low level of MHC class I is associated with poor prognosis and resistance to checkpoint blockade therapies. However, there is no technology to specifically induce MHC class I to date. Here, we show an approach for robust and specific induction of MHC class I by targeting an MHC class I transactivator (CITA)/NLRC5, using a CRISPR (clustered regularly interspaced short palindromic repeats)/Cas9-based gene-specific system, designated TRED-I (Targeted reactivation and demethylation for MHC-I). The TRED-I system specifically recruits a demethylating enzyme and transcriptional activators on the *NLRC5* promoter, driving increased MHC class I antigen presentation and accelerated CD8+ T cell activation. Introduction of the TRED-I system in animal cancer model exhibited tumor suppressive effects accompanied with increased infiltration and activation of CD8+ T cells. Moreover, this approach boosted the efficacy of checkpoint blockade therapy using anti-PD1 (Programmed cell death protein) antibody. Therefore, targeting *NLRC5* by this strategy provides an attractive therapeutic approach for cancer.

Significance Statement:

MHC class I molecules is a key player in human immune system and critical for detection and elimination of cancer cells. Although it has been known that augmented MHC class I expression is beneficial for cancer therapy, there has been no drug or technology to specifically induce MHC class I. Here, we report specific and robust induction of MHC class I expression in cancer by applying a modified CRISPR/Cas9 technology for enhancement of the expression of MHC class I transactivator, also known as NLRC5. NLRC5 induction activated anti-cancer immunity, reduced tumor volume, and enhanced efficacy of checkpoint blockade therapy. Therefore, targeting NLRC5 using this technology is a promising cancer therapeutic approach.

Main Text

Introduction

Antigen presentation through MHC class I is critical for recognition and eradication of cancers by CD8+ T cells. While cytotoxic CD8+ T cells are equipped with strong tumor killing activity through cytotoxic molecules such as perforin or granzymes (1), cancer cells evolve to evade CD8+ T cell mediated anti-cancer immunity by various strategies for successful survival, replication and growth (2). Downregulation of MHC class I gene expression is one of the major immune evasion mechanisms observed in cancer (3). Moreover, the efficacy of immune checkpoint blockade (ICB) therapy, such as anti-PD-1 therapy, is only 20~30% and the impaired MHC class I expression is considered as one of the major mechanisms underlying this resistance (4-10).

An MHC class I transactivator (CITA), NLRC5 functions as a master transcriptional regulator of MHC class I and related genes (11, 12). Genetic and epigenetic alteration of *NLRC5* is associated with cancer immune evasion and reduced responses to ICB therapy. NLRC5 interacts with multiple transcription factors on the promoters of MHC class I and related genes and generates the large protein/DNA complex termed the MHC class I enhanceosome complex, which transcriptionally activates genes encoding MHC class I and other key molecules, including proteasome, transporter, and MHC class I subunit B2M (13). *Nlrc5* deletion causes reduced expression of MHC class I and related genes and impaired CD8+ T cell-mediated killing of target cells in mice (14-17). In cancer patients, the expression level of *NLRC5* is positively correlated with MHC class I expression and patients' prognosis (18). Additionally, the expression level of *NLRC5* in cancer patients is positively correlated with responsiveness to anti-PD-1 therapy (19). The *NLRC5* promoter is frequently and aberrantly methylated in various cancers (18). The DNA methylation level of the *NLRC5* promoter is negatively correlated with expression levels of *NLRC5*, MHC class I genes, and patients' prognosis (18). Although demethylation of the *NLRC5* promoter is an attractive therapeutic target to enhance host anti-cancer immunity by upregulation of the expression of *NLRC5* and MHC class I genes, existing DNA demethylating drugs such as 5-Aza have limited clinical applicability due to severe side effects including bone marrow suppression (20).

In this study, we have developed a novel immunotherapeutic approach using targeted demethylation and activation of the *NLRC5* promoter. We developed modified CRISPR/Cas9 system that contains a demethylating enzyme and transcriptional activators (TRED-I; Targeted Reactivation and Demethylation for MHC class I). The TRED-I system robustly and specifically enhanced MHC class I-dependent immune responses and the efficacy of anti-PD-1 treatment in a murine model of melanoma. Our results highlight targeting *NLRC5* by the TRED-I system as an

attractive therapeutic approach, which may be effectively used in combination with other cancer immunotherapies.

Results

Targeted demethylation of the *Nlrc5* promoter in B16F10 increased *Nlrc5* expression

NLRC5 promoter methylation status is negatively correlated with the MHC class I gene expression and infiltration of CD8+ T cells (18). We hypothesized that demethylation of the *NLRC5* promoter in cancer provides a potential therapeutic approach that promote immune cell infiltration by increasing the expression of *NLRC5* and dependent MHC class I and related genes. Consistent with previous reports (18), the *NLRC5* promoter was hypermethylated in melanoma and breast carcinoma (Fig. S1A,B), and the *NLRC5* methylation level was negatively correlated with the expression of *NLRC5*, infiltration of immune cells including CD8+ T cell, and its activation marker *GZMB* expression (Fig. 1A, Fig. S1C,D,E) (21). Therefore, we selected a poorly immunogenic mouse melanoma B16F10 cell line, which carries low MHC class I expression levels for experimentally interrogating the role of methylation in cancer resistance (22). Upon bisulfite sequencing, we found that the *Nlrc5* promoter was significantly methylated in B16F10 cells (Fig. 1B).

To induce targeted demethylation in the *Nlrc5* promoter, we utilized a modified CRISPR/Cas9 system, in which catalytically dead Cas9 (dCas9) is recruited to the *Nlrc5* promoter in single-guide RNA (sgRNA) sequence-specific manner (23). The catalytic domains of a Tet methylcytosine dioxygenases (TET1cd) were appended to the system through fusion with dCas9 or MS2 coat protein, which binds to aptamer sites included in the sgRNA (Fig. 1C). The multiple copies of TET1cd in the system were expected to efficiently induce site-specific DNA demethylation. The modified system is referred to as the TD-I (Targeted Demethylation for MHC class I) system (Fig. 1C). Similar approaches have successfully induced targeted demethylation (24-27).

We stably transduced the TD-I system into B16F10 cells and named the stable cell line as B16F10-TD-I. We optimized *Nlrc5*-targeting sgRNA by quantifying *Nlrc5* mRNA induction by each sgRNA. Non-targeting scrambled sgRNA was transduced as control, which was referred to as sgScramble. SgRNA #4 elicited the highest level of *Nlrc5* mRNA and was referred to as sg*Nlrc5* (Fig. 1D). We confirmed successful demethylation of the *Nlrc5* promoter as methylated cytosines were completely removed in TD-I-sg*Nlrc5* cells (Fig. 1E). Quantification of mRNA levels by qRT-PCR showed that TD-I-sg*Nlrc5* expressing cells exhibited increased levels of *Nlrc5*. Increased mRNA levels were also observed in *Nlrc5*-dependent MHC class I and related genes, including *H2-K^b*, *H2-D^b, Psmb9*, *Tap1*, and *B2m* (Fig. 1F). However, similar increases were not observed for *Ciita* in the presence of IFN-γ stimulation (Fig. 1G). To characterize the transcriptome profile, we performed RNA-seq analysis on TD-I-sgScramble and TD-I-sg*Nlrc5* cells, and identified *Nlrc5* as one of the significantly

upregulated genes (Fig. 1G, Datasets S1). We also confirmed that surface MHC class I levels were upregulated on TD-I-sg*Nlrc5* cells with or without IFN-γ stimulation (Fig. 1H, Fig. S2A).

Next, we examined whether tumor immunogenicity was increased in TD-I-sg*Nlrc5* cells. B16F10-TD-I sgScramble and sg*Nlrc5* cells were loaded with the ovalbumin (OVA) peptide and co-cultured with OVA-specific OT-I CD8+ T cells. TD-I-sg*Nlrc5* cells showed higher proportions of activated IFN-γ+ and CD69+ OT-I T cells when loaded with high doses of OVA peptide (Fig. 1I; Fig. S2B; Fig. S3A). These results indicate that demethylation of the *Nlrc5* promoter can upregulate MHC class I expression with modest increases of tumor immunogenicity towards CD8+ T cells in the B16F10 model.

Targeted demethylation and activation of *Nlrc5* enhanced B16F10 immunogenicity.

Since demethylation of the *Nlrc5* promoter in B16F10 cells resulted in only modest increases in tumor immunogenicity, we sought to enhance *Nlrc5* transactivation by adding transcriptional activators to the TD-I system. Three transcriptional activators, VP64, P65, and HSF1, were appended to the TD-I system, which was referred to as the TRED-I system (Fig. 2A). Recruitment of these activators to target genes by the CRIPSR/dCas9 system were shown to induce robust and specific gene activation (28). We stably transduced the TRED-I system into B16F10 cells and then generated a B16F10-TRED-I cell line. Non-targeting control sgRNA, sgScramble or *Nlrc5* targeting sgRNA, sg*Nlrc5* were also stably transduced into B16F10-TRED-I cells. The specific demethylation of the *Nlrc5* promoter in B16F10-TRED-I was confirmed by bisulfite PCR with reduced methylated cytosines only adjacent to the sg*Nlrc5* targeting site (Fig. 2B; Fig. S4A; Fig. S5B). qRT-PCR analysis of TRED-I-sg*Nlrc5* cells showed increased mRNA levels of *Nlrc5* and *Nlrc5*-dependent MHC class I and related genes, including *H2-K^b*, *H2-D^b, Psmb9*, *Tap1*, and *B2m,* but not of an unrelated *Mx1* gene, compared to TRED-I-sgScramble cells (Fig. 2C). RNA-seq analysis showed that *Nlrc5* and *Nlrc5*-dependent MHC class I and related genes comprised most of the significantly highly expressed genes in TRED-I-sg*Nlrc5* cells. However, the expression of Nlrc5-independent transcription factors *Stat1* and *Irf1* (29) was not upregulated in TRED-I-sg*Nlrc5* cells, confirming the specificity of the TRED-I system (Fig. 2D, Fig. S5A, Datasets S1). Surface H2-K^b, H2-D^b, and H2-K^b/D^b levels, evaluated by flow cytometry, were also significantly upregulated on TRED-I-sg*Nlrc5* cells (Fig. 2E; Fig. S2A).

It has been shown that DNA methylation may affect histone acetylation status through the recruitment of methyl-DNA binding proteins and activity of histone deacetylases (HDACs) (30-32) To ask if histone acetylation status is affected by demethylation of the *Nlrc5* promoter, we performed ChIP-qPCR for TD-I and TRED-I sgScramble and sg*Nlrc5* cells using an anti-acetyl histone H3 antibody (Fig. S5B). Histone H3 acetylation levels were significantly increased in the location adjacent to *sgNlrc5* targeting site in the *Nlrc5* promoter (*Nlrc5* Exon 1). A similar increase was observed in the H2-D^b promoter in TD-I and TRED-I sg*Nlrc5* cells, as well as the H2-K^b

promoter in TRED-I cells compared to sgScramble controls. However, corresponding increases were not observed in locations distant from sg*Nlrc5* in the *Nlrc5* locus (*Nlrc5* Exon 23) or the *Gapdh* promotor (Fig. S5C). These data indicate that TD-I-dependent demethylation of the *Nlrc5* promoter induced histone H3 acetylation at the local promoter site, as well as at the MHC class I locus, possibly due to the upregulation of NLRC5, which co-operates with histone acetyl transferases (HATs) (12).

Next, we investigated whether tumor immunogenicity was increased in TRED-I-sg*Nlrc5* cells by co-culturing with OT-I CD8+ T cells after loading them with OVA peptide. Compared to OT-I CD8+ T cells co-cultured with TRED-I-sgScramble cells, OT-I T cells with TRED-I-sg*Nlrc5* cells exhibited increased activation accompanied with higher frequency in IFN-γ+ and CD69+ cells even at low doses (0.125 μg ml^{-1}) of OVA peptide (Fig. 2F; Fig. S2B; Fig. S3B). Cell death assays showed higher specific killing of TRED-I-sg*Nlrc5* cells by OT-I CD8+ T cells than TRED-I-sgScramble cells in an OVA peptide dose-dependent manner (Fig. 2G; Fig. S2C; Fig. S3C). To confirm that antigen presentation of endogenous antigens was also increased in TRED-I-sg*Nlrc5* cells, we first immunized female C57BL/6 mice with whole tumor lysates of TRED-I cells, expecting expansion of endogenous antigen-specific CD8 T cells against male tissue-specific antigens and neoantigens from male-derived B16F10 melanoma. Subsequently, CD8+ T cells were harvested and co-cultured with TRED-I sgScramble and sg*Nlrc5* cells (Fig. S6A). CD8+ T cells co-cultured with TRED-I-sg*Nlrc5* cells showed an increased proportion of IFN-γ+ and CD69+ CD8+ T cells compared with the sgScramble control (Fig. S6B,C), suggesting the increased immunogenicity against both exogenous peptide and endogenous antigens in the TRED-I-sg*Nlrc5* cells. Altogether, these results demonstrate that targeted demethylation and activation by the TRED-I-sg*Nlrc5* system induced robust transcriptional activation of *Nlrc5* and downstream MHC class I, resulting in enhanced tumor immunogenicity to CD8+ T cells.

CD8+ T cell-mediated anti-cancer immunity is enhanced by targeted demethylation and activation of *Nlrc5*

Since TRED-I-sg*Nlrc5* cells showed enhanced immunogenicity, we asked whether the TRED-I system augment anti-cancer immunity *in vivo*. We subcutaneously implanted B16F10-TRED-I sgScramble and sg*Nlrc5* cells into C57BL/6 mice. Tumor growth of TRED-I-sg*Nlrc5* cells was significantly delayed compared with sgScramble control (Fig. 3A,B). To identify whether the transcription of *Nlrc5*, MHC class I and related gene is upregulated in TRED-I-sg*Nlrc5* tumors *in vivo*, RNA-seq analysis was performed using total RNA extracted from tumors. Differentially expressed gene analysis identified that genes involved in the MHC class I antigen presentation pathway, including *Nlrc5*, *H2-D1*, *Psmb9*, *Tap1*, *B2m*, as well as cytotoxic CD8+ T cell activation markers, including *Gzmb,* were significantly upregulated in TRED-I-sg*Nlrc5* tumors (Fig. 3C; Fig. S4B; Datasets S1), while a proliferation marker *Mki67* was significantly downregulated (Fig. 3C;

Datasets S1). The gene ontology enrichment analysis showed that pathways related to antigen presentation and adaptive immune responses were among the top upregulated pathways in TRED-I-sg*Nlrc5* tumors (Fig. 3D, Datasets S2).

Next, to characterize tumor infiltrating cells, flow cytometry was performed (Fig. S2D,E). We observed increased CD45+ hematopoietic cells in TRED-I-sg*Nlrc5* tumors (Fig. 3E; Fig. S7A), accompanied with increased CD8+, but not CD4+ T cells (Fig. 3E; Fig. S7B). Tumor-infiltrating CD8+ T cells exhibited higher frequencies of activation marker IFN-γ+ (33) and effector/memory marker CD44+ (34, 35) populations in TRED-I-sg*Nlrc5* tumors, indicating increased numbers of activated CD8+ T cells (Fig. 3E; Fig. S7C,D). The increased infiltration and activation of CD8+ T cells in TRED-I-sg*Nlrc5* tumors is likely associated with elevated surface H2-K^b/D^b (Fig. 3F), leading to effective tumor cell killing, evidenced by significant decreases in live tumor cells (Fig. 3E; Fig. S7E).

To determine whether the adaptive immune system and CD8+ T cells are required to inhibit tumor growth in sg*Nlrc5* tumors, we subcutaneously implanted B16F10-TRED-I sgScramble and sg*Nlrc5* tumors into NUDE mice, which lack mature T cells, or C57BL/6 mice depleted of CD8+ T cells. Tumor growth was similar between TRED-I sgScramble and sg*Nlrc5* tumors in both NUDE mice and the CD8+ T cells-depleted mice, indicating critical roles of CD8+ T cell-dependent adaptive immunity in inhibiting sg*Nlrc5* tumor growth (Fig. 3G, H, I, J, Fig. S7F). Altogether, these results indicate that targeted demethylation and activation of *Nlrc5* led to poor tumor growth *in vivo*, accompanied with augmented MHC class I expression and increased CD8+ T cell infiltration and activation.

CD8+ T cells were preferentially recruited into the tumor center upon demethylation and activation of *Nlrc5*

Since localization of tumor-infiltrating lymphocytes (TILs) in the tumor center correlates with better cancer patients' prognoses and responses to immune checkpoint blockade therapy (36, 37), we histopathologically examined the localization of TILs. TRED-I-sg*Nlrc5* tumors displayed abundant immune cell infiltration upon H&E staining (Fig. 4A), with increased infiltration of CD3+ and CD8+ T cells in both the centers and margins of tumors following immunohistochemistry (Fig. 4A,B; Fig. S8A,B; Fig. S9A,B). Upon quantification of the percentages and the ratio of CD3+ or CD8+ stained areas in the center and margin of the same tumor, we found that CD8+ T cell infiltration was more concentrated in the center of TRED-I-sg*Nlrc5* tumors compared with sgScramble tumors,

suggesting that demethylation and activation of the *Nlrc5* promoter may not only impact the recruitment of TILs but drive the infiltration of CD8+ T cells into the center of tumors (Fig. 4B,C).

Targeted demethylation and activation of *Nlrc5* sensitized B16F10 cells to anti-PD-1 treatment

We previously found that higher expression of *NLRC5* in melanoma is correlated with better responses to anti-PD-1 checkpoint blockade therapy (19). Since the TRED-I system robustly induced *Nlrc5* expression, we hypothesized that TRED-I-sg*Nlrc5* tumors are more sensitive to anti-PD-1 treatment. To test this, we subcutaneously implanted twice the amount (6×10^5) of B16F10-TRED-I sgScramble and sg*Nlrc5* tumors into the mice compared with previous experiments (Fig. 3A,B) and treated with anti-PD-1 or isotype control antibodies. Increased transplanted tumor cell numbers led to faster tumor growth, avoiding complete elimination by enhanced anti-cancer immunity, ensuring characterization of TILs. Although anti-PD-1 treatment significantly reduced the tumor volume of both TRED-I-sgScramble and sg*Nlrc5* tumors, we observed the lowest tumor volume in TRED-I-sg*Nlrc5* tumors with anti-PD-1 treatment (Fig. 5A,B). We harvested TRED-I sgScramble tumors on day 15 and sg*Nlrc5* tumors on day 18 when their tumor volumes were similar to those of isotype control-treated tumors (Fig. 5B). While the weights of TRED-I-sgScramble and sg*Nlrc5* tumors were not significantly different with isotype control treatment at these time points, weights of TRED-I-sg*Nlrc5* tumors were significantly reduced compared with sgScramble tumors with anti-PD-1 treatment (Fig. 5C). These results suggest that B16F10-TRED-I sg*Nlrc5* tumors respond more efficiently to anti-PD-1 treatment.

Similarly, flow cytometry was performed to characterize tumor-infiltrating cells (Fig. S2D,E). TRED-I-sg*Nlrc5* tumors treated by anti-PD-1 showed the highest levels of infiltrating CD45+ hematopoietic cells, together with CD8+, but not CD4+ T cells (Fig. 5D; Fig. S10A,B). IFN-γ+ and CD44+ CD8+ T cells were robustly augmented in TRED-I-sg*Nlrc5* tumors treated by anti-PD-1, while only no or mild increases of IFN-γ+ and CD44+ CD4+ T cells were observed (Fig. 5D; Fig. S10C,D). Increased CD8+ T cell infiltration and activation in TRED-I-sg*Nlrc5* tumors treated by anti-PD-1 is likely to be associated with elevated surface H2-K^b/D^b, but not surface PD-L1 levels (Fig. 5E). Taken together, our results indicate that targeted demethylation and activation of *Nlrc5* enhanced the response to anti-PD-1 treatment by increasing the immunogenicity to CD8+ T cells through upregulation of MHC class I.

Targeted demethylation and activation of *Nlrc5* may induce anti-cancer immunity against distant tumors.

It has been long observed that local therapies, such as radiation, may induce therapeutic effects on distant tumors through altered immune responses, known as the abscopal effect (38, 39). We wondered whether robust anti-cancer immunity induced by the TRED-I system could induce similar

effects against distant tumors. To address this question, we established a bilateral tumor model, where TRED-I sgScramble and sg*Nlrc5* cells were implanted in the opposite flanks and the mice were treated with isotype or anti-PD-1 antibodies (Fig. S11A). Sizes and weights of TRED-I sg*Nlrc5* tumors tended to be smaller than TRED-I sgScramble tumors in both isotype- and anti-PD-1-treated groups (Fig. S11B,C,D), suggesting that the TRED-I system induced anti-tumor activity. To highlight the effect of the TRED-I system on the tumor in the opposite flank, we compared the tumor volume of the unilateral model (Fig. 5B) and the bilateral model (Fig. S11C) on day 15 side by side (Fig. S11E,F). The volumes of sg*Nlrc5* tumors in the unilateral model were significantly smaller than sgScramble tumors in both isotype-treated and anti-PD-1-treated groups. However, there was no significant difference in the volume between sg*Nlrc5* tumors and sgScramble tumors in the bilateral model. This is largely due to the smaller volumes of sgScramble tumors in the bilateral model than the unilateral model in both isotype-treated (unilateral / bilateral model = 0.65x fold) and anti-PD-1-treated groups (unilateral / bilateral model = 0.59x fold) (Fig. S11F), while the volumes of sg*Nlrc5* tumors in the bilateral model tended to be similar to unilateral model in both isotype-treated (unilateral / bilateral model = 1.11x fold) and anti-PD-1-treated group (unilateral / bilateral model = 0.76x fold) (Fig. S11F). These data indicate that the TRED-1 system may impact not only the local tumor but also distant tumors on the opposite flanks, possibly through elicitation of robust anti-tumor immune responses.

Targeted demethylation and activation of *NLRC5* increased MHC class I expression levels in human breast cancer cells.

Next, we asked whether a strategy based on the targeted demethylation and activation of *Nlrc5* can be applied to human cancer. We used the human breast cancer cell line MCF7 for these studies as it has low *NLRC5* expression and high methylation levels according to the NCI60 database (40) (Fig. S4C). We identified a highly methylated region in the *NLRC5* promoter in MCF7 cells upon bisulfite sequencing (Fig. 6A). To target the methylated region, we stably transduced the TRED-I system into the MCF7 cell line and optimized targeting sgRNA on the human *NLRC5* promoter by quantifying *NLRC5* expression. All 6 sgRNA candidates induces *NLRC5* expression at modest level (Fig. 6B). To enhance the *NLRC5* activation efficiency, we transduced combinations of multiple sgRNAs into MCF7-TRED-I. Among the combinations tested, a combination of sgRNA #1 + #2 + #3 showed the highest *NLRC5* induction (Fig. 6C), which is referred to as MCF7-TRED-I sg*NLRC5s*. Non-targeting scrambled sgRNA was used as control, referred to as MCF7-TRED-I sgScramble. The methylation levels of the *NLRC5* promoter were decreased in sg*NLRC5s* cells (Fig. 6D; Fig. S4D). The mRNA expression levels of *NLRC5* and dependent MHC class I and related gene, including *HLA-A, B, C, PSMB9, TAP1*, and *B2M* but not of *CIITA* were induced by sg*NLRC5s* (Fig. 6E). The surface MHC class I levels determined by antibodies against HLA-A2, HLA-B or HLA-A, B, C were increased in TRED-I-sg*NLRC5s* cells (Fig. 6F). These results suggest

that the TRED-I system can induce targeted demethylation and activation of human *NLRC5* gene, resulting in the increased expression of MHC class I in human breast cancer cells.

Discussion

In this study, we showed that targeted demethylation and activation of the *Nlrc5* promoter robustly upregulate MHC class I, accompanied by enhanced CD8+ T cell-mediated anti-cancer immunity. Demethylation of *Nlrc5* was highly specific, as shown by bisulfite sequencing and bisulfite PCR (Fig. 1E; Fig. 2B; Fig. 6D, Fig. S5B). Coupling *Nlrc5*-specific demethylation with transactivation led to the robust induction of MHC class I-dependent immune responses, highlighted by increased *NLRC5* expression at the mRNA level (Fig. 2C,D), upregulated MHC class I at the transcript and protein levels (Fig. 2C,D,E), enhanced CD8+ T cell responses *ex vivo* and *in vivo* (Fig. 2F,G; Fig. 3C,D,E; Fig. 4; Fig. S4B) and increased anti-tumor effects *in vivo* (Fig. 3A,B; Fig. 5A,B; Fig. S11B,C,D).

Enhancing MHC class I-dependent antigen presentation has been widely appreciated as a promising cancer therapeutic approach because downregulation of MHC class I is one of the most common causes for cancer immune evasion (41). Although DNA demethylating agents have been known to enhance cancer immunogenicity (42), these agents are not specific to the MHC class I antigen presentation pathway, providing severe side effects that limit their clinical applications (20). Furthermore, drugs including HDAC (histone deacetylases) inhibitors (43), STING agonists (44), and type I interferon (45) were shown to possess anti-cancer activity partially due to their ability to induce MHC class I in cancer. However, these approaches are also accompanied with low specificity and substantial side effects (46-48). To our knowledge, our strategy is the first to display the specific induction of the expression of MHC class I and related genes in cancer, which makes the *Nlrc5*-specific TRED-I system an attractive approach for developing novel cancer immunotherapies.

While the subcutaneous B16F10 model is known to elicit only poor responses to anti-PD-1 treatment (49-54), B16F10-TRED-I sg*Nlrc5* tumors showed enhanced responses to anti-PD-1 treatment (Fig. 5, Fig. S11), consistent with observations that loss of MHC class I expression correlates with resistance to anti-PD-1 therapy (4, 6-10). In addition to anti-PD-1 therapy, our results suggest that *NLRC5* can be targeted to augment the efficacy of various immunotherapies. For example, CAR T cell therapy against solid tumors may fail due to the immune-suppressing tumor microenvironment (55) and difficulty in trafficking and infiltrating into tumors (56). We found that CD8+ T cells were more abundant, activated, and concentrated in the center of TRED-I-sg*Nlrc5* tumors (Fig. 3E; Fig. 4). These histopathological data for CD8+ T cells suggest that targeting *Nlrc5* could augment CAR T cell therapeutic efficacy. Furthermore, dendritic cells (DCs) and peptide-

based anti-cancer vaccination can induce cancer antigen-specific T cell responses (57, 58), but the downregulation of MHC class I levels in cancer cells may inhibit its effectiveness. Targeting *NLRC5* together with DCs and peptide-based vaccine could augment its efficacy by restoring MHC class I antigen presentation in cancer.

The introduction of *Nlrc5*-dependent TRED-I system exerted efficient anti-tumor immunity by CD8+ T cells. This is perhaps mediated by both direct activation of CD8+ T cells and indirect recruitment due to increased availability of cancer-specific antigens to antigen-presenting cells because of cytotoxicity. However, there were unexpected additional effects that may have also contributed to tumor suppression. First, the TRED-I and TD-I system induced favorable histone H3 acetylation status in the promoter of *Nlrc5* and MHC class I (Fig. S5C). Since it has been demonstrated that methyl-DNA binding proteins, such as MeCP2, selectively bind methylated CpG dinucleotides and recruit HDACs (30), the TRED-I and TD-I system may increase the MHC class I gene expression by suppressing the locus-specific HDAC activity in addition to DNA demethylation of the *Nlrc5* promoter. Second, CD8+ T cells were efficiently recruited into the center of the tumor (Fig. 4C). Although the molecular mechanism behind this is not clear, it may provide additional therapeutic effects since it has been shown that increased numbers of CD8+ T cells in the tumor center serve as a strong biomarker for preferable prognosis in solid cancer patients (59). Third, it is likely that the TRED-I system may exert therapeutic effects on distant tumors (Fig. S11), possibly through the elicitation of robust anti-cancer immune responses. This may suggest possible clinical applications of the TRED-I system on metastatic tumors. It would be of interest to understand if these effects sum up during treatment.

We consider the direct delivery of the TRED-I system into cancer cells as an ideal approach. However, the complexity of the TRED-I system may hinder its delivery. Recently developed delivery approaches that exploit lipid nanoparticles or virus-like particles have been shown to provide highly efficient delivery of complexes of mRNA and proteins *in vivo* (60, 61). Such technologies may enable delivery of the TRED-I system efficiently *in vivo*. Alternatively, injection of liquid nitrogen snap frozen cancer cells *in vivo* were shown to increase host anti-cancer immune response (62, 63). As a potential therapeutic approach, TRED-I-introduced cancer cells can be generated *ex vivo*, followed by snap freezing and injection into the host, with the expectation that the enhanced MHC class I expression levels stimulated by the TRED-I system may induce stronger anti-cancer responses through diverse mechanisms, including DC cross dressing (64, 65).

In conclusion, we show that targeted demethylation and activation of *Nlrc5* by the TRED-I system is an attractive approach to increase MHC class I, highlighting *Nlrc5* as a cancer immunotherapy target. Further research may develop novel therapeutics with specific induction of the MHC class

l-dependent antigen presentation pathway, which may be combined with other immunotherapies to boost therapeutic efficacy.

Materials and Methods

B16F10 and MCF7 cells were obtained from RIKEN Bio BRC, Japan. Lenti-X 293T cells were obtained from Takara Bio. TD-I and TRED-I system were integrated into B16F10 and MCF7 cells by lentiviral vector transduction. Assessment of DNA methylation level, quantitative reverse transcription-PCR, flow cytometry, *ex vivo* CD8+ T cell and tumor cell co-culture, and *in vivo* tumor model were performed as described previously (24, 65, 66). For detailed Material and Methods, see SI Appendix, Materials and Methods.

Data, Materials, and Software Availability

DNA methylation and RNA-Seq gene expression data from TCGA SKCM and BRCA were accessed through UNSC XENA at https://xenabrowser.net/datapages/ (67-69). RNA-Seq generated in this study is deposited to GEO at https://www.ncbi.nlm.nih.gov/geo/ and can be accessed through GSE233194. Codes used for RNA-Seq data process and part of figures were deposited to GitHub at https://github.com/firemanzzzz/Demethylation_Nlrc5.

Acknowledgments

The authors thank C. Matsukawa and K. Ogawa for secretarial assistance, Tsutomu Tanaka for editing and all members of the Department of Immunology of the Graduate School of Medicine at Hokkaido university for their support. This work was supported by Japan Society for the Promotion of Science (JSPS) KAKEN grant 19K21250, 20K21511, 22H02883, 22KK0112; Japan Agency for Medical Research and Development (AMED) grant JP223fa627005 and 23ym0126801j0002; Japan Science and Technology (JST) START University Ecosystem Promotion Type grant JPMJST2284; Takeda Science Foundation; Bristol Myers Squibb; SENSHIN Medical Research Foundation; Hitachi Global Foundation; Kobayashi Foundation; The Toyo Suisan Foundation (all to K.S.K.); KAKEN grant 20K16433 (T.W); 19K16681 (R.O); X.S. is the recipient of a fellowship DX Doctoral Fellowship grant PH8D220001, PH8D220009. P.d.F. receives support from the Roy Blunt NextGen Precision Health Endowment.

References

1. Trapani JA & Smyth MJ (2002) Functional significance of the perforin/granzyme cell death pathway. *Nature Reviews Immunology* 2(10):735-747.

2. Shklovskaya E & Rizos H (2021) MHC Class I Deficiency in Solid Tumors and Therapeutic Strategies to Overcome It. *Int J Mol Sci* 22(13).
3. Cornel AM, Mimpen IL, & Nierkens S (2020) MHC Class I Downregulation in Cancer: Underlying Mechanisms and Potential Targets for Cancer Immunotherapy. *Cancers* 12(7).
4. Kalbasi A & Ribas A (2020) Tumour-intrinsic resistance to immune checkpoint blockade. *Nat Rev Immunol* 20(1):25-39.
5. Le DT*, et al.* (2017) Mismatch repair deficiency predicts response of solid tumors to PD-1 blockade. *Science* 357(6349):409-413.
6. Sade-Feldman M*, et al.* (2017) Resistance to checkpoint blockade therapy through inactivation of antigen presentation. *Nat Commun* 8(1):1136.
7. Zaretsky JM*, et al.* (2016) Mutations Associated with Acquired Resistance to PD-1 Blockade in Melanoma. *N Engl J Med* 375(9):819-829.
8. Gettinger S*, et al.* (2017) Impaired HLA Class I Antigen Processing and Presentation as a Mechanism of Acquired Resistance to Immune Checkpoint Inhibitors in Lung CancerAntigen-Processing Defects and Resistance to PD-1 Blockade. *Cancer Discov.* 7(12):1420-1435.
9. Chowell D*, et al.* (2018) Patient HLA class I genotype influences cancer response to checkpoint blockade immunotherapy. *Science* 359(6375):582-587.
10. Rodig SJ*, et al.* (2018) MHC proteins confer differential sensitivity to CTLA-4 and PD-1 blockade in untreated metastatic melanoma. *Sci Transl Med* 10(450):eaar3342.
11. Meissner TB*, et al.* (2010) NLR family member NLRC5 is a transcriptional regulator of MHC class I genes. *Proc Natl Acad Sci U S A* 107(31):13794-13799.
12. Meissner TB*, et al.* (2012) NLRC5 cooperates with the RFX transcription factor complex to induce MHC class I gene expression. *J Immunol* 188(10):4951-4958.
13. Kobayashi KS & van den Elsen PJ (2012) NLRC5: a key regulator of MHC class I-dependent immune responses. *Nature Reviews Immunology* 12(12):813-820.
14. Biswas A, Meissner TB, Kawai T, & Kobayashi KS (2012) Cutting edge: impaired MHC class I expression in mice deficient for Nlrc5/class I transactivator. *J Immunol* 189(2):516-520.
15. Robbins GR*, et al.* (2012) Regulation of class I major histocompatibility complex (MHC) by nucleotide-binding domain, leucine-rich repeat-containing (NLR) proteins. *J Biol Chem* 287(29):24294-24303.
16. Yao Y*, et al.* (2012) NLRC5 regulates MHC class I antigen presentation in host defense against intracellular pathogens. *Cell Res* 22(5):836-847.
17. Staehli F*, et al.* (2012) NLRC5 deficiency selectively impairs MHC class I- dependent lymphocyte killing by cytotoxic T cells. *J Immunol* 188(8):3820-3828.
18. Yoshihama S*, et al.* (2016) NLRC5/MHC class I transactivator is a target for immune evasion in cancer. *Proc Natl Acad Sci U S A* 113(21):5999-6004.
19. Yoshihama S*, et al.* (2021) NLRC5/CITA expression correlates with efficient response to checkpoint blockade immunotherapy. *Sci Rep* 11(1):3258.
20. Nguyen J*, et al.* (2021) Phase I trial of 5-aza-4'-thio-2'-deoxycytidine (Aza-TdC) in patients with advanced solid tumors. *Journal of Clinical Oncology* 39(15_suppl):3088-3088.
21. Prakash MD*, et al.* (2014) Granzyme B promotes cytotoxic lymphocyte transmigration via basement membrane remodeling. *Immunity* 41(6):960-972.

22. Wang J, Saffold S, Cao X, Krauss J, & Chen W (1998) Eliciting T Cell Immunity Against Poorly Immunogenic Tumors by Immunization with Dendritic Cell-Tumor Fusion Vaccines1. *The Journal of Immunology* 161(10):5516-5524.
23. Qi Lei S*, et al.* (2013) Repurposing CRISPR as an RNA-Guided Platform for Sequence-Specific Control of Gene Expression. *Cell* 152(5):1173-1183.
24. Liu XS*, et al.* (2016) Editing DNA Methylation in the Mammalian Genome. *Cell* 167(1):233-247 e217.
25. Liu XS*, et al.* (2018) Rescue of Fragile X Syndrome Neurons by DNA Methylation Editing of the *FMR1* Gene. *Cell* 172(5):979-992 e976.
26. Xu X*, et al.* (2016) A CRISPR-based approach for targeted DNA demethylation. *Cell Discov* 2(1):16009.
27. Choudhury SR, Cui Y, Lubecka K, Stefanska B, & Irudayaraj J (2016) CRISPR-dCas9 mediated TET1 targeting for selective DNA demethylation at BRCA1 promoter. *Oncotarget* 7(29):46545-46556.
28. Konermann S*, et al.* (2015) Genome-scale transcriptional activation by an engineered CRISPR-Cas9 complex. *Nature* 517(7536):583-588.
29. Yoo JS*, et al.* (2021) SARS-CoV-2 inhibits induction of the MHC class I pathway by targeting the STAT1-IRF1-NLRC5 axis. *Nat Commun* 12(1):6602.
30. Du Q, Luu PL, Stirzaker C, & Clark SJ (2015) Methyl-CpG-binding domain proteins: readers of the epigenome. *Epigenomics* 7(6):1051-1073.
31. Lyst MJ*, et al.* (2013) Rett syndrome mutations abolish the interaction of MeCP2 with the NCoR/SMRT co-repressor. *Nat Neurosci* 16(7):898-902.
32. Shahbazian M*, et al.* (2002) Mice with truncated MeCP2 recapitulate many Rett syndrome features and display hyperacetylation of histone H3. *Neuron* 35(2):243-254.
33. Nicolet BP*, et al.* (2020) CD29 identifies IFN-γ–producing human CD8+ T cells with an increased cytotoxic potential. *Proceedings of the National Academy of Sciences* 117(12):6686-6696.
34. Baaten BJ, Tinoco R, Chen AT, & Bradley LM (2012) Regulation of Antigen-Experienced T Cells: Lessons from the Quintessential Memory Marker CD44. *Front Immunol* 3:23.
35. Topham DJ & Reilly EC (2018) Tissue-Resident Memory CD8(+) T Cells: From Phenotype to Function. *Front Immunol* 9:515.
36. Galon J*, et al.* (2012) Cancer classification using the Immunoscore: a worldwide task force. *J Transl Med* 10(1):205.
37. Nie RC*, et al.* (2019) Robust immunoscore model to predict the response to anti-PD1 therapy in melanoma. *Aging (Albany NY)* 11(23):11576-11590.
38. Ngwa W*, et al.* (2018) Using immunotherapy to boost the abscopal effect. *Nat Rev Cancer* 18(5):313-322.
39. Whiteside TL, Demaria S, Rodriguez-Ruiz ME, Zarour HM, & Melero I (2016) Emerging Opportunities and Challenges in Cancer Immunotherapy. *Clin Cancer Res* 22(8):1845-1855.
40. Shoemaker RH (2006) The NCI60 human tumour cell line anticancer drug screen. *Nat Rev Cancer* 6(10):813-823.
41. Dersh D*, et al.* (2021) Genome-wide Screens Identify Lineage- and Tumor-Specific Genes Modulating MHC-I- and MHC-II-Restricted Immunosurveillance of Human Lymphomas. *Immunity* 54(1):116-131 e110.
42. Hogg SJ, Beavis PA, Dawson MA, & Johnstone RW (2020) Targeting the epigenetic regulation of antitumour immunity. *Nature Reviews Drug Discovery* 19(11):776-800.

43. Woan KV*, et al.* (2015) Targeting histone deacetylase 6 mediates a dual anti-melanoma effect: Enhanced antitumor immunity and impaired cell proliferation. *Molecular Oncology* 9(7):1447-1457.
44. Falahat R*, et al.* (2019) STING Signaling in Melanoma Cells Shapes Antigenicity and Can Promote Antitumor T-cell Activity. *Cancer Immunology Research* 7(11):1837-1848.
45. Palmer KJ, Harries M, Gore ME, & Collins MK (2000) Interferon-alpha (IFN-alpha) stimulates anti-melanoma cytotoxic T lymphocyte (CTL) generation in mixed lymphocyte tumour cultures (MLTC). *Clin Exp Immunol* 119(3):412-418.
46. Peng X, Sun Z, Kuang P, & Chen J (2020) Recent progress on HDAC inhibitors with dual targeting capabilities for cancer treatment. *European Journal of Medicinal Chemistry* 208:112831.
47. Le Naour J, Zitvogel L, Galluzzi L, Vacchelli E, & Kroemer G (2020) Trial watch: STING agonists in cancer therapy. *Oncoimmunology* 9(1):1777624.
48. García-Martínez E*, et al.* (2018) Trial Watch: Immunostimulation with recombinant cytokines for cancer therapy. *OncoImmunology* 7(6):e1433982.
49. Pi C*, et al.* (2022) Reversing PD-1 Resistance in B16F10 Cells and Recovering Tumour Immunity Using a COX2 Inhibitor. *Cancers (Basel)* 14(17):4134.
50. De Henau O*, et al.* (2016) Overcoming resistance to checkpoint blockade therapy by targeting PI3Kgamma in myeloid cells. *Nature* 539(7629):443-447.
51. Gao W*, et al.* (2019) Prim-O-glucosylcimifugin enhances the antitumour effect of PD-1 inhibition by targeting myeloid-derived suppressor cells. *Journal for immunotherapy of cancer* 7(1):231.
52. Meng X*, et al.* (2018) FBXO38 mediates PD-1 ubiquitination and regulates anti-tumour immunity of T cells. *Nature* 564(7734):130-135.
53. Albershardt TC*, et al.* (2020) Therapeutic efficacy of PD1/PDL1 blockade in B16 melanoma is greatly enhanced by immunization with dendritic cell-targeting lentiviral vector and protein vaccine. *Vaccine* 38(17):3369-3377.
54. Iwai Y, Terawaki S, & Honjo T (2004) PD-1 blockade inhibits hematogenous spread of poorly immunogenic tumor cells by enhanced recruitment of effector T cells. *International Immunology* 17(2):133-144.
55. Majzner RG & Mackall CL (2019) Clinical lessons learned from the first leg of the CAR T cell journey. *Nature Medicine* 25(9):1341-1355.
56. Sterner RC & Sterner RM (2021) CAR-T cell therapy: current limitations and potential strategies. *Blood Cancer Journal* 11(4):69.
57. Laureano RS*, et al.* (2022) Trial watch: Dendritic cell (DC)-based immunotherapy for cancer. *OncoImmunology* 11(1):2096363.
58. Bezu L*, et al.* (2018) Trial watch: Peptide-based vaccines in anticancer therapy. *OncoImmunology* 7(12):e1511506.
59. Galon J*, et al.* (2006) Type, density, and location of immune cells within human colorectal tumors predict clinical outcome. *Science* 313(5795):1960-1964.
60. TX M (An Efficacy Study of Adjuvant Treatment With the Personalized Cancer Vaccine mRNA-4157 and Pembrolizumab in Participants With High-Risk Melanoma (KEYNOTE-942).
61. Banskota S*, et al.* (2022) Engineered virus-like particles for efficient in vivo delivery of therapeutic proteins. *Cell* 185(2):250-265 e216.
62. Ci T*, et al.* (2020) Cryo-shocked cancer cells for targeted drug delivery and vaccination. *Sci Adv* 6(50):eabc3013.

63. Zhao Z*, et al.* (2022) Walking Dead Tumor Cells for Targeted Drug Delivery Against Lung Metastasis of Triple-Negative Breast Cancer. *Adv Mater* 34(33):e2205462.
64. MacNabb BW*, et al.* (2022) Dendritic cells can prime anti-tumor CD8(+) T cell responses through major histocompatibility complex cross-dressing. *Immunity* 55(6):982-997 e988.
65. Duong E*, et al.* (2022) Type I interferon activates MHC class I-dressed CD11b(+) conventional dendritic cells to promote protective anti-tumor CD8(+) T cell immunity. *Immunity* 55(2):308-323 e309.
66. Kasuga Y*, et al.* (2023) FBXO11 constitutes a major negative regulator of MHC class II through ubiquitin-dependent proteasomal degradation of CIITA. *PNAS* 120(24):e2218955120.
67. Goldman MJ*, et al.* (2020) Visualizing and interpreting cancer genomics data via the Xena platform. *Nat Biotechnol* 38(6):675-678.
68. Cancer Genome Atlas N (2015) Genomic Classification of Cutaneous Melanoma. *Cell* 161(7):1681-1696.
69. Koboldt DC*, et al.* (2012) Comprehensive molecular portraits of human breast tumours. *Nature* 490(7418):61-70.

Figure legends

Figure 1. Demethylation of the *Nlrc5* promoter by the TD-I system induced MHC class I expression in B16F10. (A) Correlation analysis was performed between *NLRC5* expression levels or mean *NLRC5* methylation levels and estimated immune cell infiltration scores or *GZMB* expression levels in melanoma (*n* = 471) and breast invasive carcinoma tissues (*n* = 873). *r* (Pearson correlation coefficient) value was calculated plotted as heatmap. (B) DNA methylation status of the *Nlrc5* promoter in B16F10 cells was determined by bisulfite PCR analysis. CpG dinucleotides are shown as white or black circles to represent unmethylated or methylated CpG dinucleotides. Each row represents an individual plasmid clone of total 5 clones. (C) Schematic illustrations of (Upper) main components in the lentiviral vectors of the TD-I system, and (Lower) assembled components of the TD-I system at the *Nlrc5* promoter. (D) (Upper) Scramble or *Nlrc5* promoter targeting sgRNA was stably transduced in B16F10-TD-I cells and the mRNA expression level of *Nlrc5* was quantified by qRT-PCR. Relative gene expression levels were determined by 2^(–ΔΔCT) method using *Gapdh* as a reference gene. (Lower) A schematic diagram of sgRNA targeting sites at *Nlrc5* promoter, with colored triangular signs indicating each sgRNA target site corresponding to the upper plot. (E) DNA methylation status of the *Nlrc5* promoter in B16F10-TD-I sgScramble and sg*Nlrc5* cells was determined by bisulfite PCR analysis. Ten clones were analyzed per group. Triangle sign indicates *sgNlrc5* targeting site. (F) The mRNA expression levels of *Nlrc5*, *H2-K^b*, *H2-D^b*, *Psmb9*, *Tap1*, *B2m,* and *Ciita* in B16F10-TD-I sgScramble and sg*Nlrc5* cells were quantified by qRT-PCR with or without IFN-γ stimulation. Relative gene expression levels were determined by 2^(–ΔΔCT) method using *Gapdh* as a reference gene. (G) The mRNA gene expression levels by RNA-Seq in $\log_2$(Normalized Count+1) values of B16F10-TD-I sgScramble

were compared with sg*Nlrc5* cells. Marked gene is *Nlrc5* (in red). The average from *n* = 2 is shown. (H) Surface H2-K^b/D^b expression levels in B16F10-TD-I sgScramble and sg*Nlrc5* cells were quantified by flow cytometry with or without IFN-γ stimulation. (Left) Representative histogram. (Right) Geometric MFI. (I) B16F10-TD-I sgScramble and sg*Nlrc5* cells were pulsed with 0, 1, or 2 μg ml^{-1} of OVA peptide overnight and co-cultured with OT-I T cells for 24 h. Intracellular IFN-γ and surface CD69 expression levels in OT-I T cells were quantified by flow cytometry. Values in bar plots are mean ±SD. For (D, F, H, I), *n* = 3, for (F) *n* = 2 in each group; '*n*' stands for number of biological replicates. Statistical significance was determined by unpaired two-sided student's *t*-test (D) or Fisher's LSD test (F, H, I).

Figure 2. Targeted demethylation and activation of *Nlrc5* increased immunogenicity to CD8+ T cells in B16F10. (A) A schematic illustration of main components in the lentiviral vectors of the TRED-I system (Upper), and assembled components of the TRED-I system at *Nlrc5* promoter (Lower). (B) DNA methylation status of *Nlrc5* promoter in B16F10-TRED-I sgScramble and sg*Nlrc5* cells were determined by direct sanger sequencing of bisulfite PCR product. (Upper) Methylation levels of CpG dinucleotides. (Lower) A schematic diagram of sgRNA targeting sites (green triangles) and locations of CpG dinucleotides (white circles) at *Nlrc5* promoter, corresponding to upper plot. (C) B16F10-TRED-I cells were stably transduced with lentiviral vectors expressing sgScramble and sg*Nlrc5*. The mRNA expression levels of *Nlrc5*, *H2-K^b^*, *H2-D^b^*, *Psmb9*, *B2m,* and *Mx1* in B16F10-TRED-I sgScramble and sg*Nlrc5* cells were quantified by qRT-PCR. Relative gene expression levels were determined by 2^(–ΔΔCT) method using *Gapdh* as a reference gene. (D) The mRNA gene expression levels in $\log_2$(Normalized Count+1) values of all detected genes in RNA-seq analysis of B16F10-TRED-I sgScramble cells were compared with sg*Nlrc5* cells. Marked genes are *Nlrc5* and dependent MHC class I and related genes (in red), and *Nlrc5* transcription activator *Stat1*, *Irf1*, and unrelated control *Mx1* (in blue). The average from *n* = 2 is shown. (E) Surface MHC class I expression levels in B16F10-TRED-I sgScramble and sg*Nlrc5* cells were quantified by flow cytometry using antibodies against H2-K^b, H2-D^b or H2-K^b/D^b. (F) B16F10-TRED-I sgScramble and sg*Nlrc5* cells were pulsed with 0, 0.0625, 0.125, 0.25, 0.5, or 1 μg ml^{-1} of OVA peptide overnight and co-cultured with OT-I T cells for 24 h. Intracellular IFN-γ and surface CD69 expression levels on OT-I T cells were quantified by flow cytometry. (G) CFSE-labeled B16F10-TRED-I sgScramble and sg*Nlrc5* cells were pulsed with 0 or 0.5μg ml^{-1} of OVA peptide overnight and co-cultured with OT-I T cells at OT-I:B16F10 ratio of 0:1, 1.25:1, 2.5:1, 5:1, and 10:1 for 48 h. Dead B16F10-TRED-I cells were quantified as CFSE+ Zombie dye+ by flow cytometry. Values shown are mean ±SD. For (B, C, E, F, G), *n* = 3; for (D) *n* = 2 in each group; '*n*' stands for number

of biological replicates. Statistical significance was determined by Fisher's LSD test in (B, C, F, G), unpaired two-sided student's *t*-test in (E). n.s., not significant; * $p < 0.05$; ** $p < 0.01$; *** $p < 0.001$.

Figure 3. Targeted demethylation and activation of *Nlrc5* enhanced CD8+ T cell mediated anti-cancer immunity *in vivo*. (A) Three hundred thousand of B16F10-TRED-I sgScramble and sg*Nlrc5* cells were subcutaneously implanted into left flank of C57BL/6 mice on day 0. An image of tumors on day 18 was obtained, with one mouse in the sg*Nlrc5* group that did not show tumor growth. (B) Volumes of B16F10-TRED-I sgScramble and sg*Nlrc5* tumors were estimated daily by digital caliper since day 6 using visible tumor area and the following formula: volume (mm^3) = length * width * width / 2. (C) RNA-Seq and differentially expressed gene analysis between B16F10-TRED-I sgScramble and sg*Nlrc5* tumors were performed. Red signs indicate significantly upregulated genes and blue signs indicate significantly downregulated genes in TRED-I-sg*Nlrc5* tumors. FDR, false discovery rate. (D) Gene ontology pathway enrichment analysis between B16F10-TRED-I sgScramble and sg*Nlrc5* tumors *in vivo* using RNA-seq data. Green circles represent the top significantly upregulated pathways in sg*Nlrc5* tumors. Size of circle indicates the number of genes included in the gene set. (E) Quantification of tumor infiltrating CD45+, and CD4+ or CD8+ T cells, IFN-γ+ or CD44+ T cells, and viable tumor cells from B16F10-TRED-I sgScramble and sg*Nlrc5* tumors by flow cytometry. (F) Quantification of surface H2-K^b/D^b levels on viable tumor cells from B16F10-TRED-I sgScramble and sg*Nlrc5* tumors by flow cytometry. (Left) Representative histogram. (Right) Geometric MFI of live B16F10 cells. (G) Five hundred thousand of B16F10-TRED-I sgScramble and sg*Nlrc5* cells were subcutaneously implanted into left flank of NUDE mice on day 0. An image of tumors on day 15 was obtained. (H) Volumes of B16F10-TRED-I sgScramble and sg*Nlrc5* tumors from NUDE mice were estimated as above. (I) Anti-CD8+ antibody was injected in C57BL/6 mice on day –1 and day 3 to induce CD8+ T cell depletion. On day 0, 5×10^5 of B16F10-TRED-I sgScramble and sg*Nlrc5* cells were subcutaneously implanted into left flank of C57BL/6 mice. An image of tumors on day 13 was obtained. (J) Volumes of B16F10-TRED-I sgScramble and sg*Nlrc5* tumors from CD8+ T cell depleted mice were estimated as above. Values shown are mean ±SEM in (B, H, J), and mean ±SD in (E, F). For (B, E, F), $n = 7$ (TRED-I-sgScramble tumors), $n = 6$ (TRED-I-sg*Nlrc5* tumors); For (C, D) $n = 4$ in each group; For (H), $n = 7$; For (J), $n = 6$. '*n*' stands for number of biological replicates. Statistical significance was determined by two-way ANOVA test in (B, H, J), and unpaired two-sided student's *t*-test in (E, F). n.s., not significant; * $p < 0.05$; *** $p < 0.001$.

Figure 4. Targeted demethylation and activation of Nlrc5 preferentially promoted the infiltration of CD8+ T cells into center of tumors. (A) Representative H&E staining and immunohistochemistry images of tumor center and margin of B16F10-TRED-I sgScramble and sg*Nlrc5* tumors implanted in C57BL/6 mice. Upper panels indicate H&E, IHC for CD3, and CD8,

and lower panels indicate digital visualization of CD3 and CD8 positivity using artificial red color. (B) Comparison of total area of CD3 or CD8 positivities in B16F10-TRED-I sgScramble and sg*Nlrc5* tumors discriminating tumor center and margin. Digital analysis of the proportion of CD3 or CD8 positivities against whole tumor area (%). (C) The ratio of CD3+ and CD8+ stained area between tumor center and margin within each tumor was calculated and compared between TRED-I-sgScramble and sg*Nlrc5* tumors. (B, C) The numbers show are *p*-values or fold induction of antibody-stained area in TRED-I-sg*Nlrc5* tumors compared with sgScramble tumors. Bar plots in (B, C) are mean ±SD. For (A, B, C), *n* = 6 (sgScramble tumors), *n* = 5 (sg*Nlrc5* tumors); '*n*' stands for number of biological replicates. Statistical significance was determined by Fisher's LSD test.

Figure 5. Targeted demethylation and activation of *Nlrc5* sensitized B16F10-TRED-I tumors to anti-PD-1 treatment. (A) Six hundred thousand of B16F10-TRED-I sgScramble and sg*Nlrc5* cells were subcutaneously implanted into left flank of C57BL/6 mice on day 0. Isotype control or anti-PD-1 antibodies were intraperitoneally injected every 2 days from day 3 at 250 μg/mouse for 5 times in total. Image of B16F10-TRED-I sgScramble and sg*Nlrc5* tumors harvested on day 15 and day 18 respectively were obtained. (B) Tumor volumes of B16F10-TRED-I sgScramble and sg*Nlrc5* tumors treated by isotype control or anti-PD-1 antibodies were estimated every 2 days since day 3 by digital caliper using visible tumor area and the following formula: volume (mm^3) = length * width * width / 2. (C) Tumor weight was measured and compared between day 15 for sgScramble tumors and day 18 for sg*Nlrc5* tumors treated by isotype control or anti-PD-1. (D) Quantification of tumor infiltrating CD45+, and CD4+ or CD8+ T cells, and activated/effector/memory IFN-γ+ or CD44+ T cells from B16F10-TRED-I sgScramble and sg*Nlrc5* tumors by flow cytometry. (E) Quantification of H2-K^b/D^b and PD-L1 levels on viable tumor cells from B16F10-TRED-I sgScramble and sg*Nlrc5* tumors treated by isotype control or anti-PD-1 by flow cytometry. (Left) Mean gMFI of live B16F10 cells. (Right) Representative histogram. Values shown in (A) are mean ±SEM, and in (C, D, E) are mean ±SD. *n* = 8 in each group; '*n*' stands for number of biological replicates. Statistical significance was determined by two-way ANOVA test in (B), unpaired two-sided student's *t*-test in (C), and Fisher's LSD test in (D, E). n.s., not significant; * $p < 0.05$; ** $p < 0.01$; *** $p < 0.001$.

Figure 6. Targeted demethylation and activation of *NLRC5* increase the expression of MHC class I in MCF7. (A) DNA methylation status of *NLRC5* promoter in MCF7 cells were determined by bisulfite PCR analysis. CpG dinucleotides are shown as white or black circles to represent unmethylated or methylated CpG dinucleotides. Each row represents an individual plasmid clone of total 10 clones. (B) (Upper) Scramble and *NLRC5* promoter targeting sgRNAs were stably transduced in MCF7-TRED-I cells and the mRNA expression level of *NLRC5* was quantified by qRT-PCR. (Lower) A schematic of sgRNA targeting sites at *NLRC5* promoter, with colored

triangular signs indicating each sgRNA target site corresponding to the upper plot. (C) Lentiviral vectors expressing scramble sgRNA or multiple combinations of *NLRC5* promoter targeting sgRNAs were stably transduced in MCF7-TRED-I cells and the mRNA expression level of *NLRC5* was quantified by qRT-PCR. (D) (Upper) DNA methylation status of *NLRC5* promoter in MCF7-TRED-I sgScramble and sg*NLRC5s* cells were determined by direct sanger sequencing of bisulfite PCR product. (Lower) A schematic diagram of sgRNA targeting sites (green triangles) and locations of CpG dinucleotides (white circles) at the *NLRC5* promoter, corresponding to upper plot. (E) The mRNA expression levels of *NLRC5*, *HLA-A*, *HLA-B*, *HLA-C*, *PSMB9, TAP1*, *B2M* and *CIITA* in MCF7-TRED-I sgScramble and sg*NLRC5s* cells were quantified by qRT-PCR. (F) Surface MHC class I expression levels in MCF7-TRED-I sgScramble and sg*NLRC5s* cells were quantified by flow cytometry using antibodies against HLA-A2, HLA-B or HLA-A,B,C. Relative gene expression levels in qRT-PCR analysis were determined by 2^(–ΔΔCT) method using *GAPDH* as a reference gene. Values in bar plots shown are mean ±SD. $n = 3$ in (B, C, D, E, F); '*n*' stands for number of biological replicates. Statistical significance was determined by unpaired two-sided student's *t*-test in (C, F), Fisher's LSD test in (D, E). n.s., not significant; * $p < 0.05$; ** $p < 0.01$; *** $p < 0.001$.

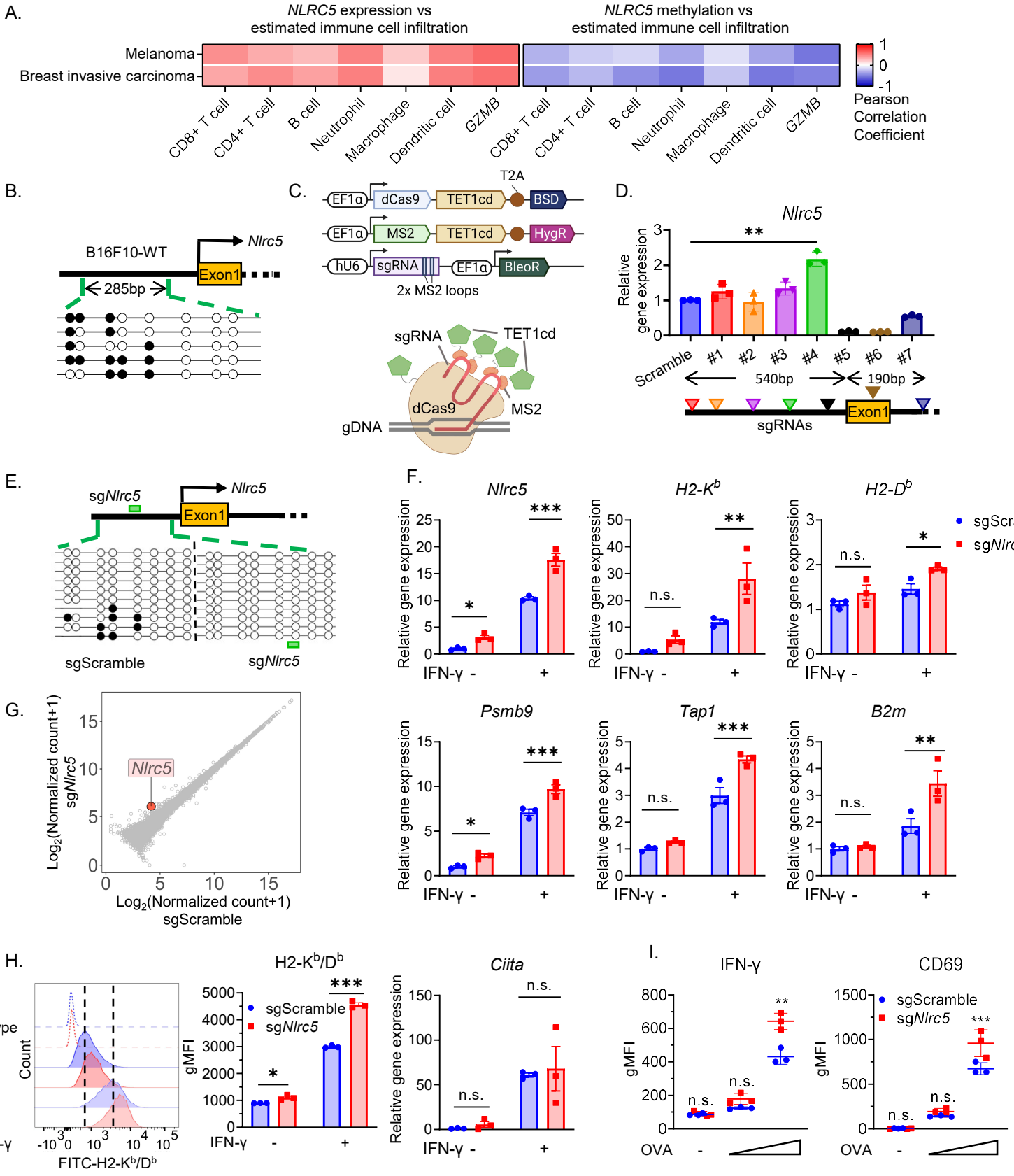
A.
NLRC5 expression vs estimated immune cell infiltration
NLRC5 methylation vs estimated immune cell infiltration
Melanoma
Breast invasive carcinoma
CD8+ T cell
CD4+ T cell
B cell
Neutrophil
Macrophage
Dendritic cell
GZMB
Pearson Correlation Coefficient
B.
B16F10-WT
Nlrc5
Exon1
285bp
C.
T2A
EF1α
dCas9
TET1cd
BSD
MS2
HygR
hU6
sgRNA
BleoR
2x MS2 loops
gDNA
D.
Nlrc5
Relative gene expression
Scramble
#1
#2
#3
#4
#5
#6
#7
540bp
190bp
sgRNAs
E.
sgNlrc5
sgScramble
F.
Nlrc5
H2-Kb
H2-Db
sgScramble
sgNlrc5
IFN-γ
G.
Log2(Normalized count+1) sgNlrc5
Log2(Normalized count+1) sgScramble
Psmb9
Tap1
B2m
H.
Isotype
Count
FITC-H2-Kb/Db
H2-Kb/Db
gMFI
Ciita
I.
IFN-γ
CD69
OVA

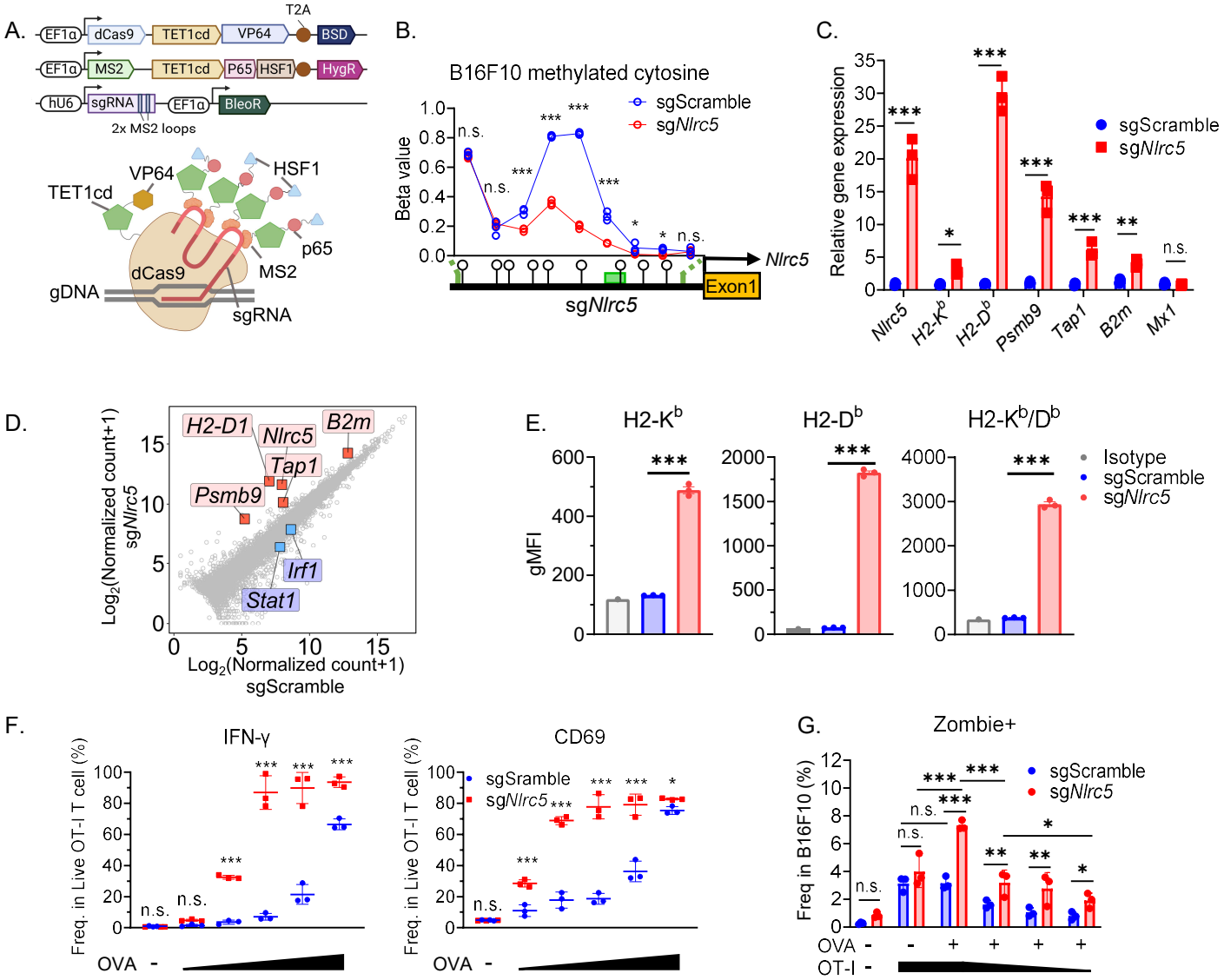
A.
EF1α
dCas9
TET1cd
VP64
T2A
BSD
EF1α
MS2
TET1cd
P65
HSF1
HygR
hU6
sgRNA
EF1α
BleoR
2x MS2 loops
TET1cd
VP64
HSF1
p65
MS2
dCas9
gDNA
sgRNA
B.
B16F10 methylated cytosine
sgScramble
sgNlrc5
Beta value
n.s.
Nlrc5
Exon1
sgNlrc5
C.
Relative gene expression
sgScramble
sgNlrc5
Nlrc5
H2-Kb
H2-Db
Psmb9
Tap1
B2m
Mx1
D.
H2-D1
Nlrc5
B2m
Tap1
Psmb9
Irf1
Stat1
Log2(Normalized count+1) sgNlrc5
Log2(Normalized count+1) sgScramble
E.
H2-Kb
H2-Db
H2-Kb/Db
gMFI
Isotype
sgScramble
sgNlrc5
F.
IFN-γ
CD69
Freq. in Live OT-I T cell (%)
sgSramble
sgNlrc5
OVA
G.
Zombie+
Freq in B16F10 (%)
sgScramble
sgNlrc5
OVA
OT-I

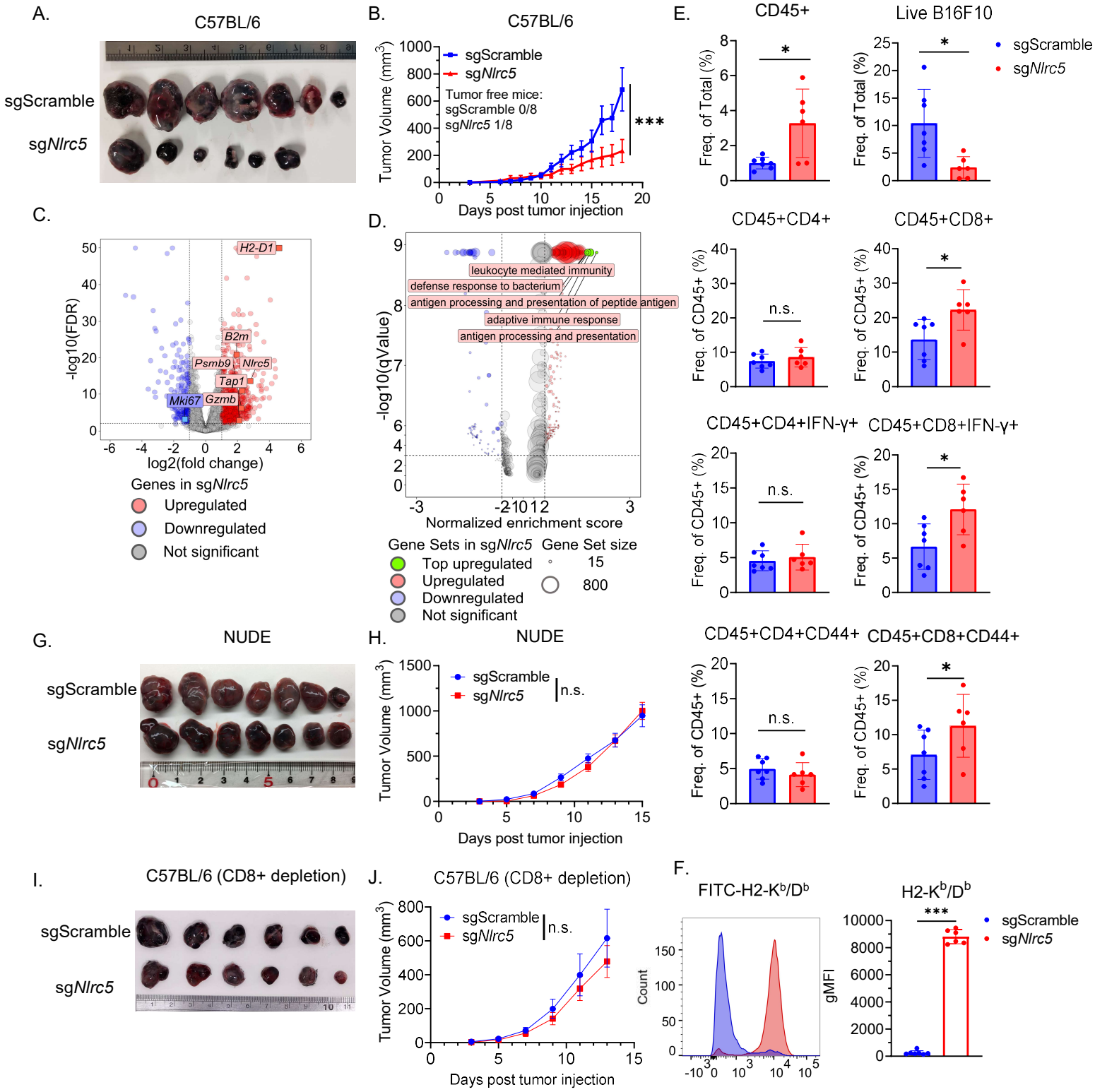
A.
C57BL/6
sgScramble
sgNlrc5
B.
C57BL/6
sgScramble
sgNlrc5
Tumor free mice:
sgScramble 0/8
sgNlrc5 1/8
***
Tumor Volume (mm3)
Days post tumor injection
E.
CD45+
Live B16F10
Freq. of Total (%)
*
C.
H2-D1
B2m
Psmb9
Nlrc5
Tap1
Mki67
Gzmb
-log10(FDR)
log2(fold change)
Genes in sgNlrc5
Upregulated
Downregulated
Not significant
D.
leukocyte mediated immunity
defense response to bacterium
antigen processing and presentation of peptide antigen
adaptive immune response
antigen processing and presentation
-log10(qValue)
Normalized enrichment score
Gene Sets in sgNlrc5
Top upregulated
Upregulated
Downregulated
Not significant
Gene Set size
15
800
CD45+CD4+
CD45+CD8+
n.s.
Freq. of CD45+ (%)
CD45+CD4+IFN-γ+
CD45+CD8+IFN-γ+
G.
NUDE
sgScramble
sgNlrc5
H.
NUDE
n.s.
CD45+CD4+CD44+
CD45+CD8+CD44+
I.
C57BL/6 (CD8+ depletion)
J.
C57BL/6 (CD8+ depletion)
F.
FITC-H2-Kb/Db
H2-Kb/Db
Count
gMFI
***

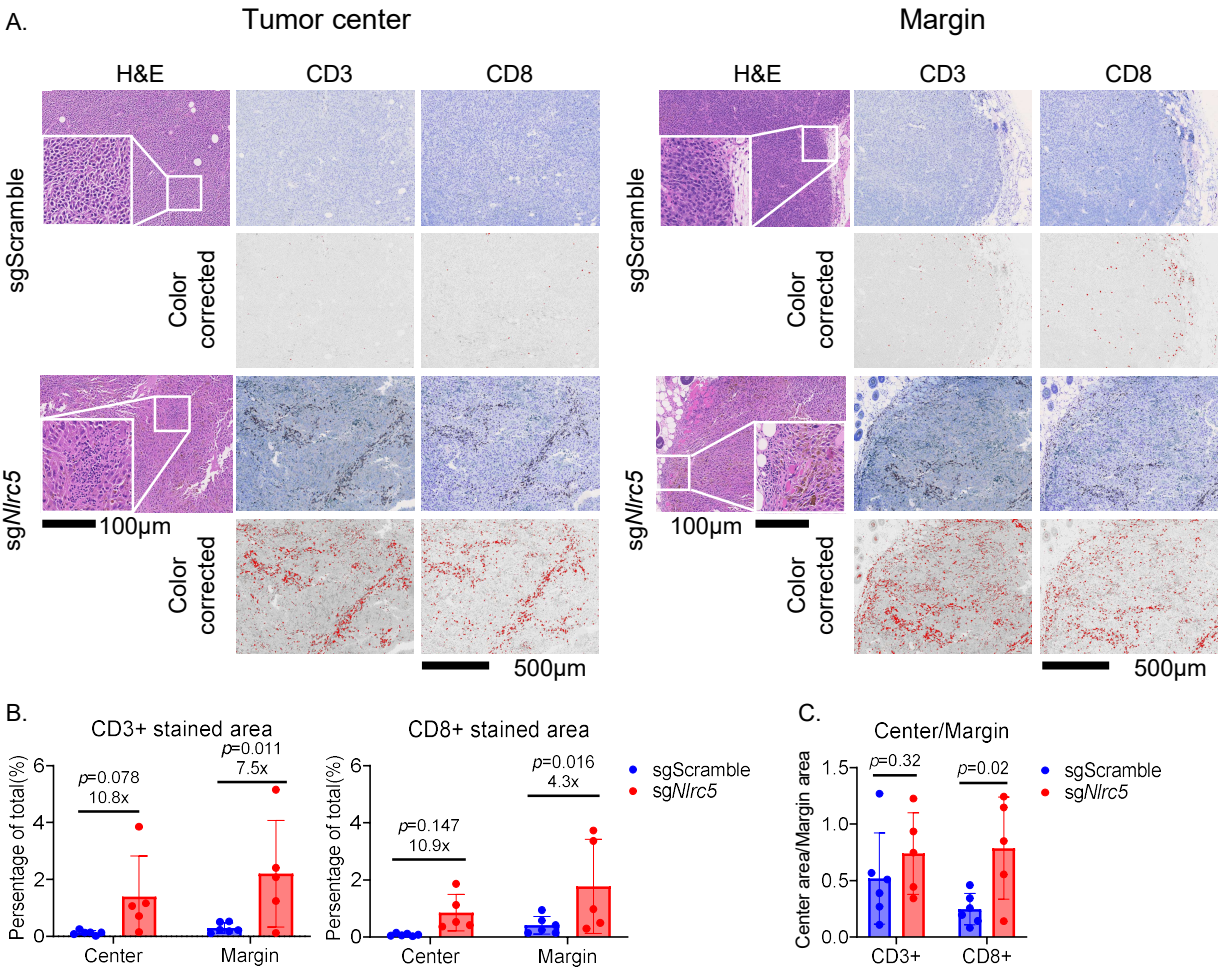
A.
Tumor center
Margin
H&E
CD3
CD8
sgScramble
sgNlrc5
Color corrected
100μm
500μm
B.
CD3+ stained area
CD8+ stained area
Persentage of total(%)
p=0.078
10.8x
p=0.011
7.5x
p=0.147
10.9x
p=0.016
4.3x
Center
Margin
sgScramble
sgNlrc5
C.
Center/Margin
Center area/Margin area
p=0.32
p=0.02
CD3+
CD8+

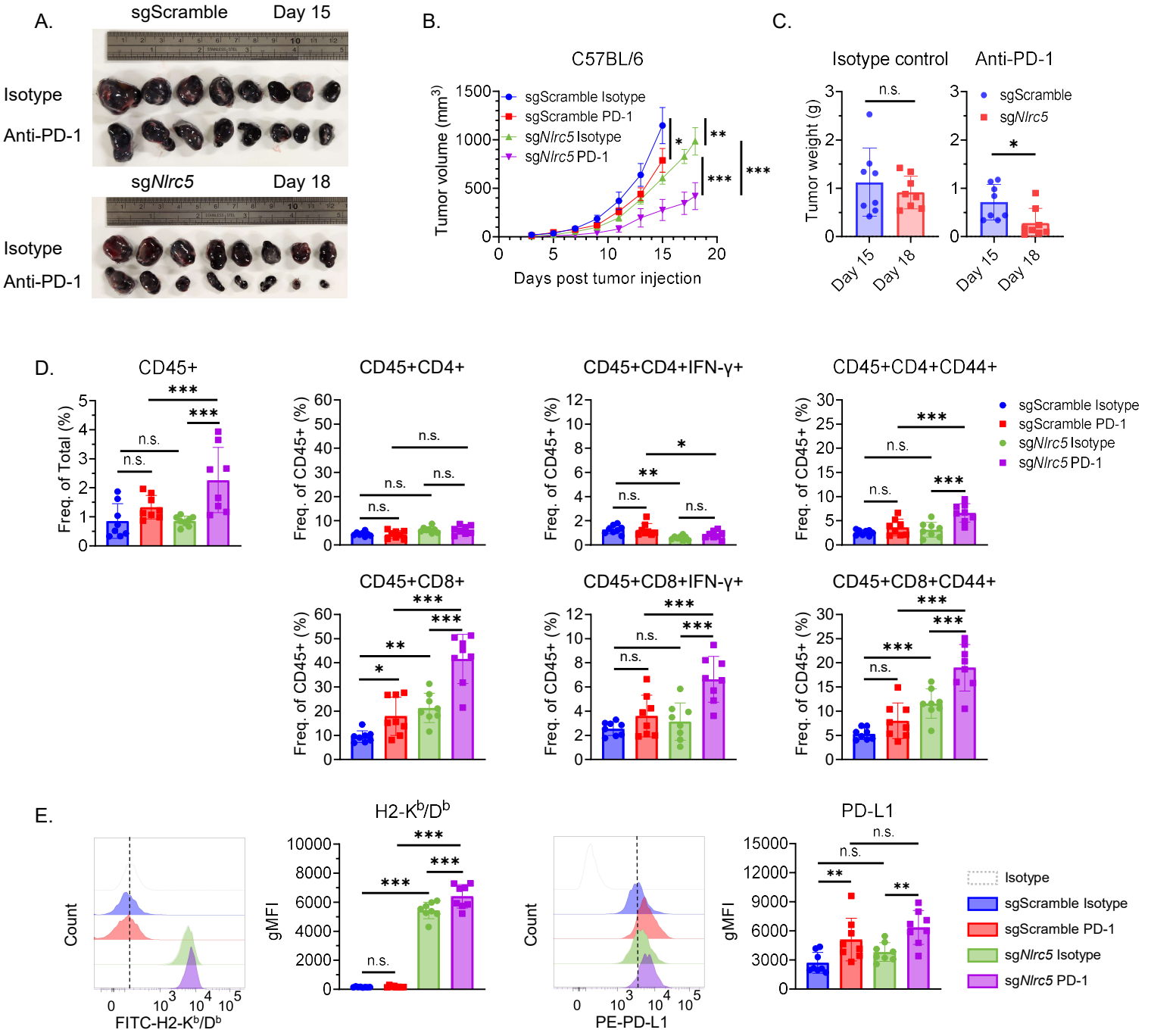
A.
sgScramble
Day 15
Isotype
Anti-PD-1
sgNlrc5
Day 18
Isotype
Anti-PD-1
B.
C57BL/6
Tumor volume (mm3)
Days post tumor injection
sgScramble Isotype
sgScramble PD-1
sgNlrc5 Isotype
sgNlrc5 PD-1
C.
Isotype control
Anti-PD-1
Tumor weight (g)
n.s.
sgScramble
sgNlrc5
Day 15
Day 18
D.
CD45+
CD45+CD4+
CD45+CD4+IFN-γ+
CD45+CD4+CD44+
CD45+CD8+
CD45+CD8+IFN-γ+
CD45+CD8+CD44+
Freq. of Total (%)
Freq. of CD45+ (%)
sgScramble Isotype
sgScramble PD-1
sgNlrc5 Isotype
sgNlrc5 PD-1
E.
H2-Kb/Db
PD-L1
Count
FITC-H2-Kb/Db
PE-PD-L1
gMFI
Isotype
sgScramble Isotype
sgScramble PD-1
sgNlrc5 Isotype
sgNlrc5 PD-1

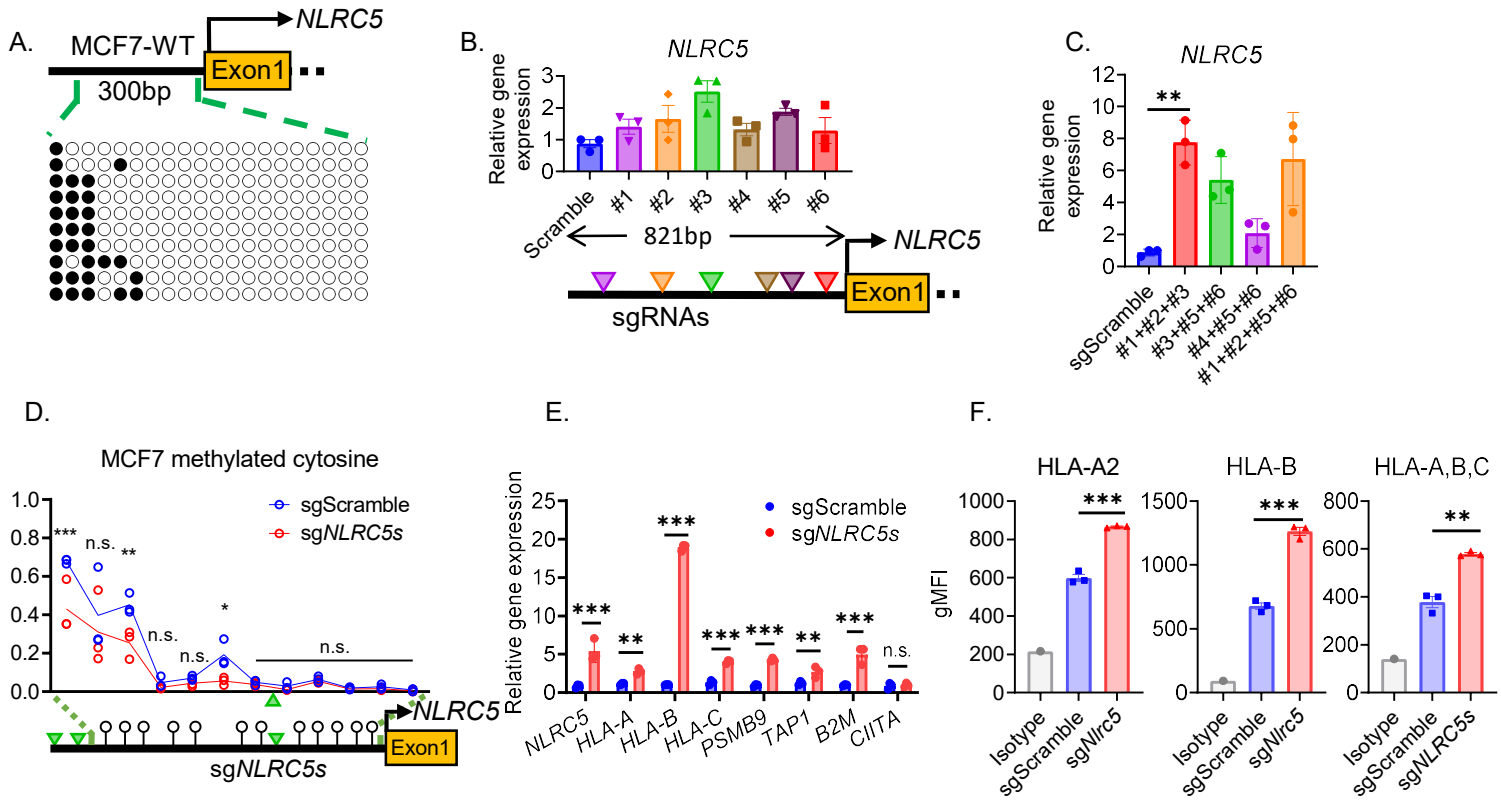
A.
MCF7-WT
NLRC5
Exon1
300bp
B.
NLRC5
Relative gene expression
Scramble
#1
#2
#3
#4
#5
#6
821bp
NLRC5
Exon1
sgRNAs
C.
NLRC5
Relative gene expression
sgScramble
#1+#2+#3
#3+#5+#6
#4+#5+#6
#1+#2+#5+#6
D.
MCF7 methylated cytosine
Beta value
sgScramble
sgNLRC5s
n.s.
NLRC5
Exon1
sgNLRC5s
E.
Relative gene expression
sgScramble
sgNLRC5s
NLRC5
HLA-A
HLA-B
HLA-C
PSMB9
TAP1
B2M
CIITA
F.
HLA-A2
HLA-B
HLA-A,B,C
gMFI
Isotype
sgScramble
sgNlrc5
sgNLRC5s